Self-excited instability occurring during the nanoparticle formation in an Ar-SiH4 low pressure radio frequency plasma

Marjorie Cavarroc, Marie Christine Jouanny, Khalid Radouane, Maxime Mikikian, Laifa Boufendi

Self-excited instability occuring during the nanoparticle formation in an Ar-SiH_4 low pressure radiofrequency plasma

M. Cavarroc,* M.C. Jouanny, K. Radouane, M. Mikikian, and L. Boufendi
GREMI-Polytech'Orléans, 14, Rue d'Issoudun, BP 6744, 45067 Orléans cedex 2, France

An experimental investigation of an instability occuring during dust nanoparticle formation is presented in this paper. The present study has been performed in radiofrequency low pressure plasmas in an argon-silane mixture. The formation and growth of nanoparticles is followed thanks to the analysis of the amplitude of the third harmonics (3H, 40.68 MHz) of the discharge current and the self bias voltage (V_{dc}). In some cases, at the end of the accumulation phase of the nanocrystallites an instability occurs. It seems to be an attachment induced-ionization instability as observed in electronegative plasmas. A detailed study of the influence of different operating conditions (injected power, gas temperature, silane flow rate) on this instability behavior and frequencies is presented. The paper concludes by examining a very particular case of the instability.

PACS numbers: 52.27.Lw, 52.35.-g, 52.70.-m

I. INTRODUCTION

In the past few years, there has been an increasing interest in dusty plasmas generated in radiofrequency (RF) discharges, and now represents one of the most rapidly growing branch of plasma physics. The range of interest spreads over both industrial plasma processing systems [1] and astrophysical plasma environments. Besides, an active research into particle formation and behavior has been induced by contamination phenomena in industrial plasma reactors used for etching, sputtering, and plasma enhanced chemical vapor deposition (PECVD). In the laboratory, two main ways are used to grow particles in rf low pressure discharges: reactive gases such as silane (SiH_4) and target sputtering by ion bombardement. In both cases a dense cloud of submicron particles is formed, tending to fill in the whole inter electrode gap.

Many theoretical [2, 3] and experimental [4, 5] studies have dealt with the detection and dynamics of particles in silane mixture discharge. In particular Boufendi and his coworkers [6], has clearly brought to the fore the way particles grow in the discharge from initial nanocrystallites (smaller than 5 nm). Presently, many studies are being carried out on nanometer size particles generated in PECVD processes, especially in the field of polymorphous silicon (pm-Si:H) deposition recently used to manufacture solar cells [7]. This new material consists of nanometer size silicon crystallites embedded in a hydrogenated amorphous silicon matrix [8–10], and shows improved transport properties and stability with respect to hydrogenated amorphous silicon. Moreover, some instabilities induced by the presence of dust particles in plasma have been reported for ten years now [11–14]. All these instabilities have been observed in particle clouds due to sputtering or particle injection. However, the instability we report in this paper, occuring in the earlier phase of the particle formation, seems to be comparable to those already reported. The phenomenon is followed through its influence on the discharge characteristics. The electrical diagnostic used in this work has been developed in the GREMI laboratory. It allows us to follow the time evolution of the amplitude of the third harmonics of the discharge current (3H) and the amplitude of the self-bias voltage (V_{dc}). This diagnostic has been shown to be able to follow the particle formation and growth in different chemistries such as silane or methane [15].

The main objective of this paper is to present our observations concerning a self-excited instability during the particle formation and growth in a silane based plasma. The effects of different parameters on this instability are also reported.

II. EXPERIMENTAL SETUP

The experimental set up used to carry out the plasma analysis has already been described in detail in previous papers [5, 16, 17]. The rf discharge is produced in a grounded cylindrical plasma box (13 cm inner diameter and 3.3 cm for inter-electrode distance). The discharge structure is surrounded by a cylindrical oven. The whole system is enclosed in a vacuum chamber. The upper electrode (driven electrode) is a shower-head one in order to ensure a homogenous gas distribution at the entrance of the plasma zone. This electrode is connected to a 13.56 MHz radiofrequency generator through a matchbox including a blocking capacitor. The power can be varied from 0 up to 20 Watts. The gas temperature is controlled from room temperature up to 150 ℃ and is measured in the gas flow just below the plasma box by a thermocouple. The current and voltage probes are inserted between the matchbox and the powered electrode. The curves are visualized on a Lecroy scope LT364L (500 MHz bandwidth and 1 GS/s) and the results are collected via a computer.

In this work, certain measurement conditions were kept constant in most cases: the argon flow rate remains 30 sccm and the total pressure is always around 12 Pa. The reference for injected power was 10 Watts corresponding to about 400 Volts peak-to-peak. The adjustment is fixed at optimal steady state conditions in argon. The current probe measures the amplitude of the third harmonics (3H) of the total current and the voltage probe gives the self-bias voltage (V_{dc}).

*Electronic address: marjorie.cavarroc@univ-orleans.fr

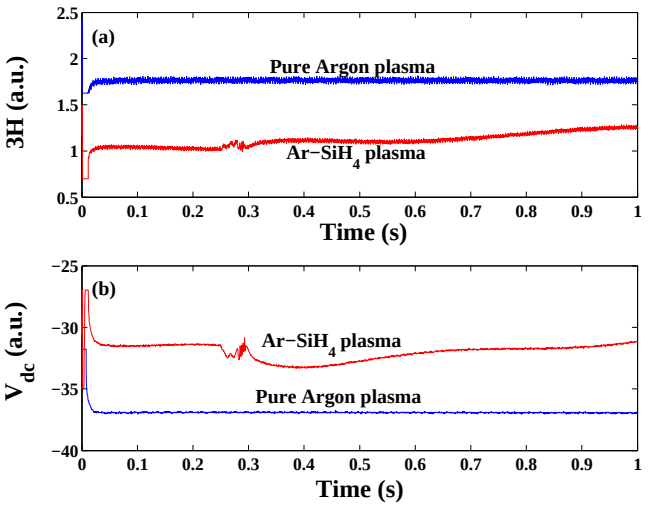

FIG. 1: (Color online) Time-evolution of the third harmonics and the self-bias voltage (a) in pure argon and (b) in argon-silane plasmas under standard conditions.

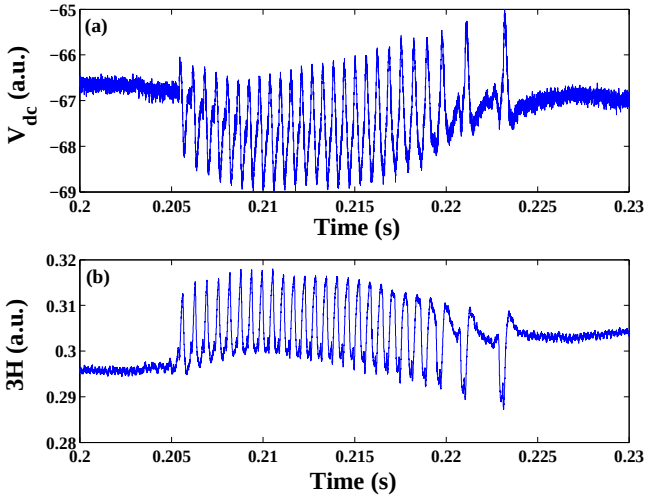

FIG. 2: (Color online) Time-evolution of the instability (a) on the self-bias voltage (b) on the third harmonics of the discharge current.

III. RESULTS AND DISCUSSION

In previous experimental and theoretical work [4, 18, 19], it has been shown that particle formation in Ar-SiH_4 low pressure plasma is a four step process. These steps are now clearly identified: growth of the nanocrystallites (2-3 nm) from molecular species, accumulation phase, fast coagulation, and growth by deposition of the plasma species on the particle surface. The growth of particles in the discharge leads to considerable modifications in the plasma characteristics. Indeed the presence of charged dust grains affects many of the physical properties of the plasma (electron density, temperature, electrical field, impedance, ...). The modification of the plasma impedance due to particle formation and growth led us to develop a diagnostic based on the measurements of the amplitude of V_{dc} and 3H. Thus, in a pure argon plasma, their amplitude remains constant in time as shown in figure 1(a). When silane is added to the the mixture, i.e. in a dust forming plasma, V_{dc} and 3H show a time evolution due to the formation and growth of dusts in the discharge (see fig.1(b)). These electrical measurements are a good diagnostic to control the particle occurence in the plasma and hence the reactor contamination. All the following observations have been performed using electrical measurements, with different operating conditions.

A. Instability

In most of our experimental conditions, we observed that an instability appears between the end of the accumulation phase and the beginning of the coalescence both on 3H and V_{dc} curves (see figure 1). The typical behavior of the self bias voltage and the third harmonics of the discharge current in this region is shown on figure 2 (for P_{RF} = 6W and Q_{SiH_4} = 0.8sccm). The frequency of this signal, given by a Fast Fourier Transform (FFT) analysis, is shown on figure 3 and evolves during the instability. We can first observe an increase of the frequency that could corresponds to the formation of the instability. Once the instability is established, the frequency decreases until the end of the phase where it becomes difficult to define the frequency. In the following, we will present some results about the frequency at the beginning and at the end of the instability. Those two frequencies are not measured in the same way. The frequency at the beginning is the average value of the frequency taken on the six first periods, whereas the frequency at the end is given by the last value of the FFT, with an uncertainty range due to the software used to compute the data.

It is known that during the coalescence phase, the particle density decreases while the particle radius and mass increase because of the coalescence of the nanocrystallites. Scanning electron microscopy (SEM) analyses of nanoparticles deposited at three different times: just before, at the beginning and in the middle of the instability, have been performed. Just before the instability, only nanocrystallites are observed (around 2 nm). At the beginning and in the middle of the instability, there are both nanocrystallites and small aggregates. These results confirm that the beginning of the instability corresponds to the beginning of the coalescence phase. Therefore,

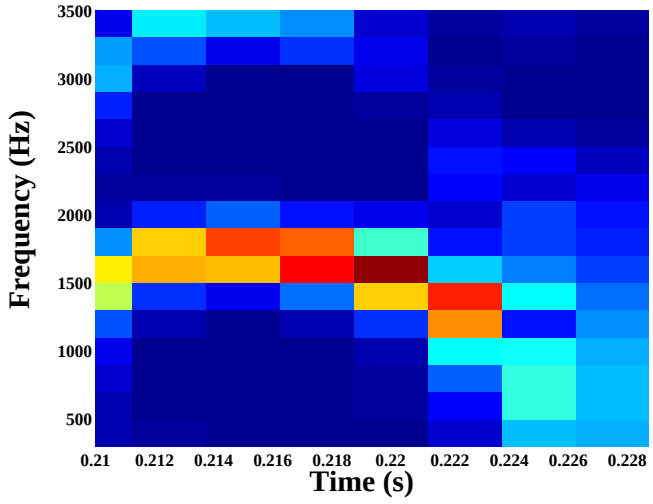

FIG. 3: (Color online) Time-evolution of the frequency of the instability.

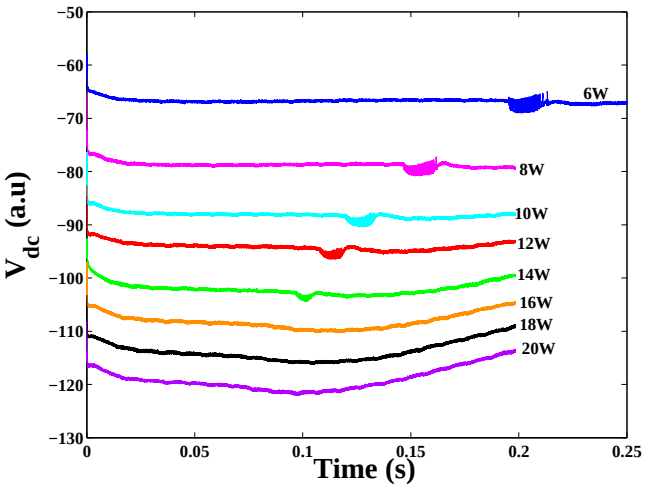

FIG. 4: (Color online) Time-evolution of the self-bias voltage versus the injected power.

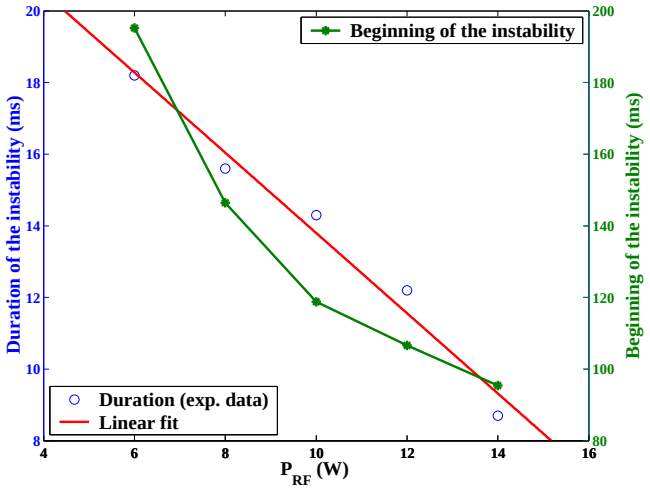

FIG. 5: (Color online) Beginning and duration of the instability as a function of the injected power.

during the instability, there is an increase in the mean mass of dust particles. The increase of the particle mass could explain the decrease of the instability frequency since when a plasma is instantaneously disturbed from its equilibrium, collective motions appear. They are characterized by a frequency of oscillations called the plasma frequency ω_p. This frequency is not the same for electrons, ions and dust but depends on the mass, charge and density of the plasma particles [20]. Dust particles oscillate around their equilibrium position with the dust plasma frequency $\omega_{pd} = \sqrt{\frac{Q_p^2 N_p}{\epsilon_0 m_p}}$ where Q_p and N_p are respectively the particle mean charge and the particle density. Assuming N_p to be the critical particle density ($10^{12} cm^{-3}$) [6], $Q_p \approx 10^{-3} e$ and 1 nm $\leq r_p \leq$ 2 nm for silicon particles [2], we get 1 kHz$\leq f_{pd} \leq$ 3 kHz (assuming $f_{pd} = \omega_{pd}/2\pi$). These frequencies correspond to the ones we observed for the instability in different conditions.

The SEM analysis of depositions made at the end of the instability shows that most of the deposited dust particles are small aggregates. At the same time, we observe a drastic decrease in the electron density due to the attachment and to the increase in the ionization rate ($\alpha - \gamma$ ' transition) [2].

B. Parameter effect

As for the different phases of particle formation and growth, the region of the instability is affected by different discharge parameters such as injected power, silane flow rate or gas temperature.

1. *Effect of the injected power*

The effect of the injected power has been studied for different gas mixture rates of Ar/SiH_4 with silane flow rate varying from 0.4 sccm up to 1.6 sccm. The following observations correspond to a synthesis of all the results obtained. Figure 4 shows the time evolution of the self bias voltage for different injected powers. In this particular case, the amount of silane in the gas mixture was relatively small (Q_{SiH_4} = 0.8 sccm), as when the silane flow rate is too high, the instability rapidly disappears when injected power is increased, and no pertinent study can be done. In this case, the instability appears only for low powers between 6 W and 14 W. For higher silane flow rate, the instability tends to disappear around 10 W. When the power is increased in the discharge, all the phases of particle formation and growth become shorter and so does the instability (see fig.5). This is due to the fact that increasing the injected power increases the ionization process, thus increasing the electron density. Consequently the formation of the particles becomes faster. The instability also starts earlier for high injected power as shown in figure 5. The amplitude of the instability also decreases when power increases. For high injected power the kinetics is very fast leading to the disappearance of the instability. The frequency of the instability has been shown to evolve in time, decreasing between the beginning and the end of the phase. In addition, the frequency at the beginning and at the end seem to depend linearly on the injected power (see fig.6). Indeed, assuming that at the end of the accumulation phase r_p and N_p are constant whatever the injected power, then ω_{pd} is proportional to the parti-

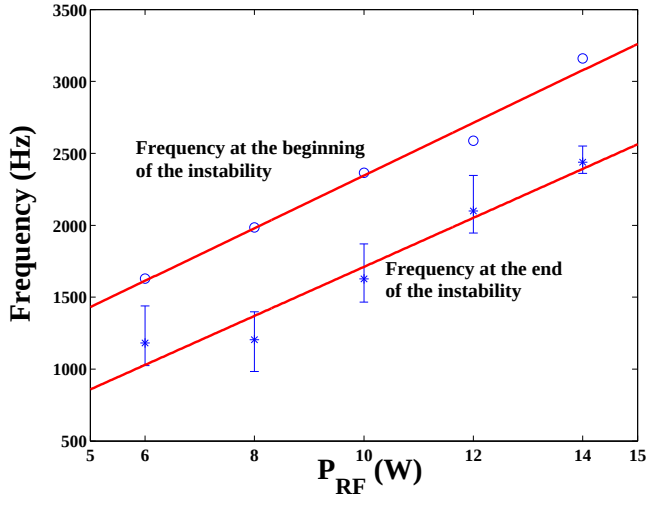

FIG. 6: (Color online) Frequency at the beginning and at the end of the instability as a function of the injected power.

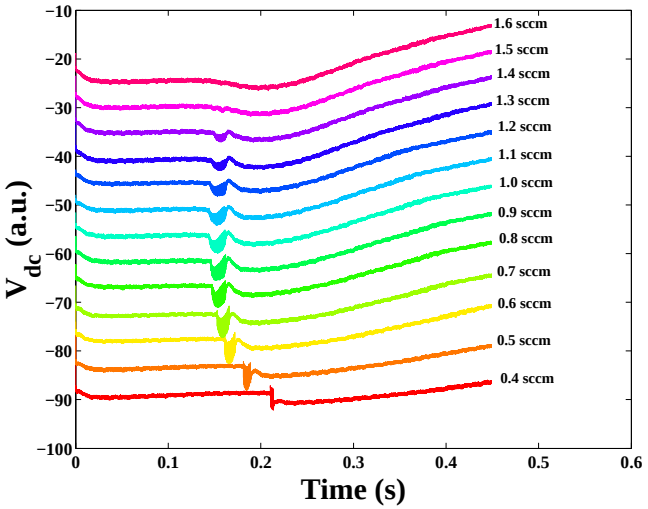

FIG. 7: (Color online) Time-evolution of the self bias voltage versus the silane flow rate. The curves are shifted on the self bias voltage axis in order to have a better overview.

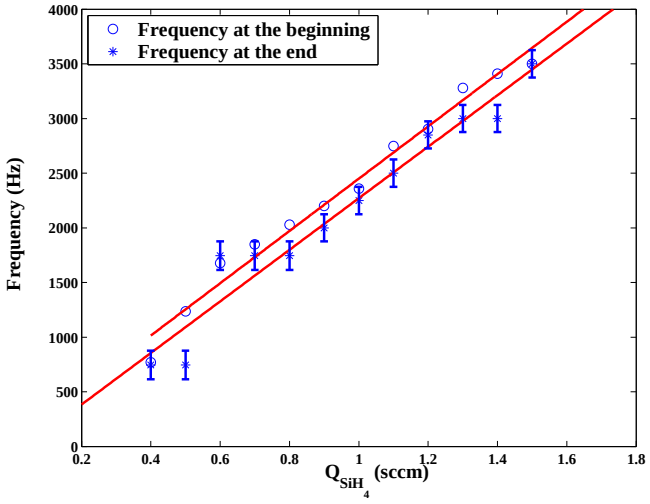

FIG. 9: (Color online) Frequency at the beginning and at the end of the instability as a function of the silane flow rate.

cle charge Q_p. The instability frequency evolves linearly with the RF power. Between 6 W and 20 W, the electron temperature remains constant (around 2 eV before the $\alpha - \gamma$' transition). Hence when the injected power is increased, the particle mean charge also increases.

2. *Effect of the silane flow rate*

The effects of the silane flow rate have been studied in an Argon/Silane plasma with an injected power of 10 W. The amount of Silane in the discharge was varied from 0.4 sccm up to 1.6 sccm, keeping all the other parameters constant. The induced pressure variation is negligible ($\sim$ 3-4 μbar) with respect to the total pressure (p $\approx$ 120 μbar). Figure 7 shows the time evolution of the self-bias voltage as a function of the silane flow rate in the discharge. The curves are shifted in the self-bias axis in order to give a better overview. In the case we present here, the injected power is low, since, as it has been shown before, when the injected power is too high, no instability can be observed. For 10 W injected power, the instability appears even for very small flow rates and tends to disappear for silane flow rates higher than 1.5 sccm. The instability duration is maximum for 1 sccm silane flow rate as shown in figure 8. From 0.4 sccm to 1 sccm the duration of the instability increases when silane flow rate is increased (see fig.8). For silane flow rate higher than 1 sccm, the instability is increasingly short until it disappears. However, overall the amplitude of the instability seems to decrease when increasing silane flow rate, until it becomes undetectable on the curves. For silane flow rates comprised between 0.4 sccm and 1 sccm, the instability was observed to begin earlier when increasing the flow rate. From 1 sccm, this value seems to increase slightly until the disappearance of the phenomenon (see fig.8). When the quantity of silane in the discharge is increased, the amount of precursors is increased. Indeed, the dissociation degree of silane is constant and independent of the silane flow rate [21]. The initial, accumulation and coagulation phases are therefore quicker. The silane flow rate acts on chemical reactions in the discharge. However it seems that above a given limit (around 1 sccm in our case) an equilibrium is reached, and the reactions are no longer speed up. The frequency of the instability has been shown to have a time evolution. Figure 9 shows the evolution of the frequency at the beginning and at the end of the instability as a function of the silane flow rate. These two frequencies seem to depend linearly on the amount of silane in the discharge.

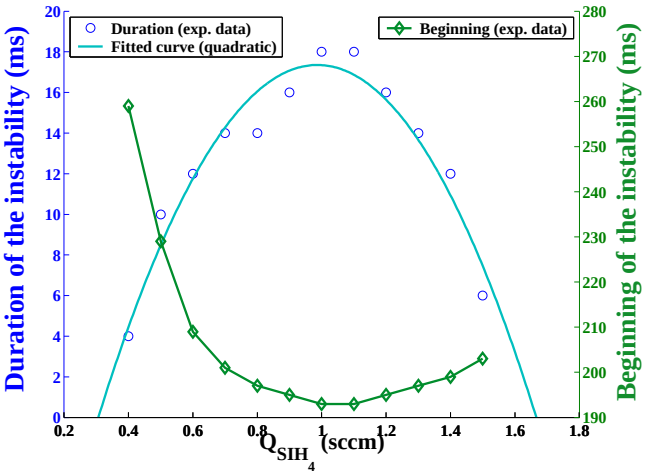

FIG. 8: (Color online) Beginning and duration of the instability as a function of the silane flow rate.

3. *Effect of the temperature*

The influence of the gas temperature on particle formation and growth was the subject of many papers [4, 22–25]. When the gas temperature is increased, particle formation is delayed. In this work, the influence of the gas temperature has been studied from room temperature (RT) up to 120°C (measured in the gas flow with a thermocouple just below the plasma box) at constant gas number density. We observed that the instability region is also affected by the temperature. Figure 10 shows the time evolution of the self-bias voltage versus the gas temperature. The curves are shifted in the self-bias axis in order to have a better overview.

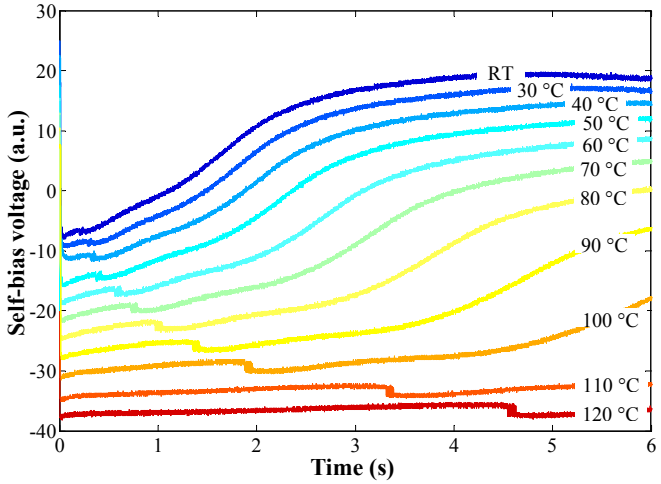

FIG. 10: (Color online) Time-evolution of the self-bias voltage versus the temperature. The curves are shifted on the self bias voltage axis in order to have a better overview.

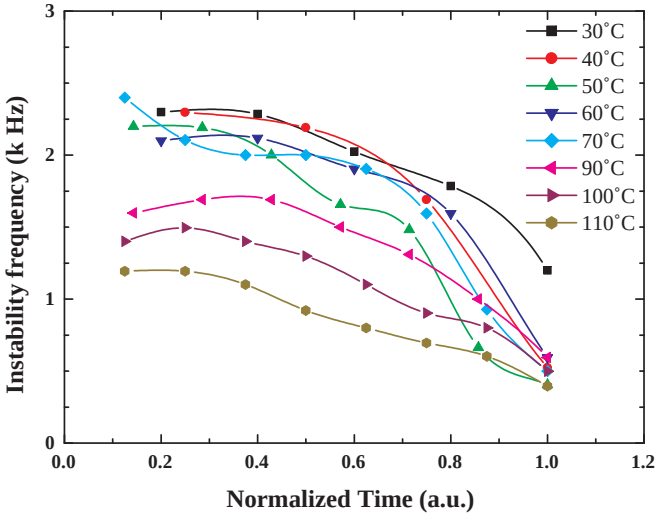

FIG. 12: (Color online) Time-evolution of the frequency of instability versus the temperature. The time scale has been normalized by the instability duration to have a significant overview.

When the temperature is increased, the appearance of the instability is delayed (see fig 11). The duration of the instability is also affected by the gas temperature: the higher the temperature, the longer the instability (fig.11). The instability behaves like the different phases of particle formation and growth: it is delayed and it lasts longer when the temperature is increased. Figure 12 shows the time evolution of the instability frequency as a function of the gas temperature. The time scale has been normalized by the instability duration in order to give a good overview of the evolution. The frequency at the beginning decreases as the temperature increases, while the frequency at the end remains the same at around 0.6 kHz (except on the curve taken at 30°C). This last point suggests that the frequency at the end of the instability could be linked to the particle density in the plasma. In fact, the end of the instability could correspond to the beginning of the coalescence phase that cannot start unless the critical particle density value ($10^{11} - 10^{12}$ cm^{-3}) has been reached.

4. *Particular case of the instability*

In some very specific conditions a particular case of the instability was observed. The figure 13 shows the shape of the instability in this case. In a first part, it behaves in the same way as the "common" instability, then it finishes before briefly restarting. This has been confirmed by a frequency analysis (FFT analysis) (see fig.14). We can observe a time evolution of the frequency and a range of frequencies similar to those previously observed (between 2 kHz and 3 kHz). The second part seems to be a sort of replica of the end of the first part, with exactly the same frequencies. This phenomenon is highly sensitive to the operating conditions, appearing only for very low injected power (around 6 W) and in a very tight range of silane flow rates (several appearances between 2 and 3 sccm). Moreover, a temperature variation of only a few degrees Celsius leads to the disappearance of the phenomenon. This particular case of the instability seems to correspond to dust critical formation conditions, as

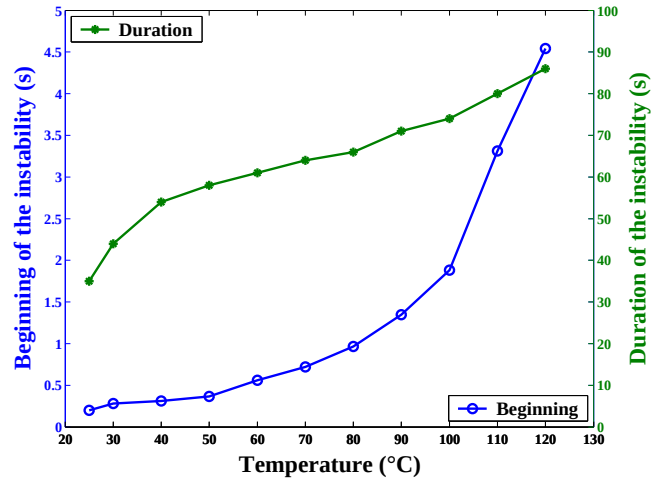

FIG. 11: (Color online) Beginning and duration of the instability as a function of the gas temperature.

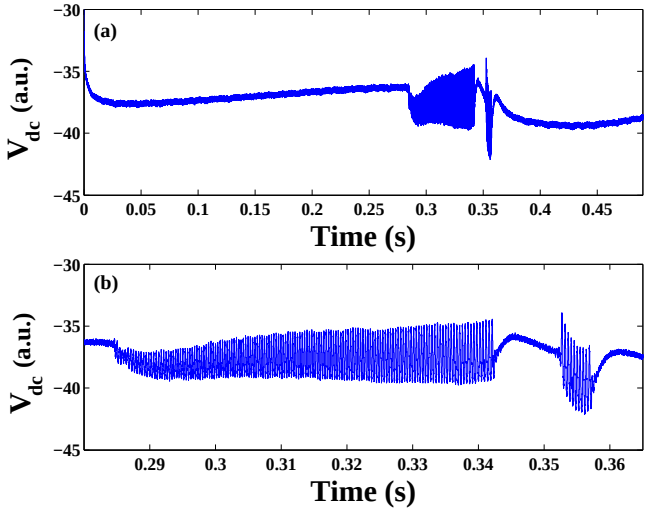

FIG. 13: (Color online) Particular case of the instability on the self-bias voltage (a) on the plasma duration (b) zoom.

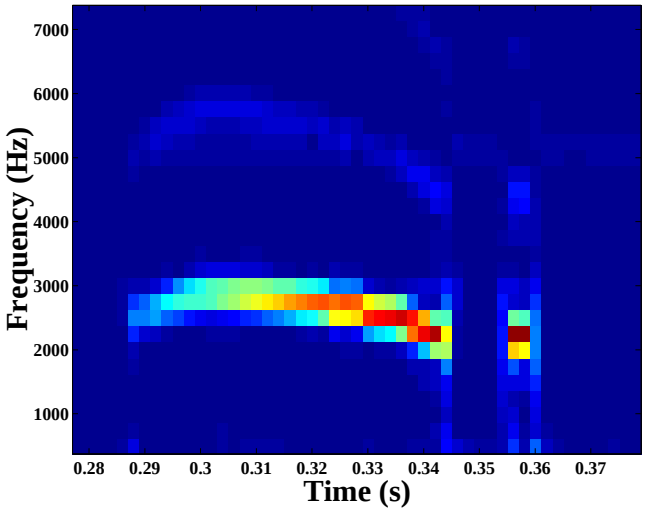

FIG. 14: (Color online) Time-evolution of the frequency of the instablity in the particular case.

the slightest modification of one of the parameters leads to the disappearance of the phenomenon. However, we observed this particular instability in at least two different sets of parameters. This observation leads us to surmise that a special pair particle density/particle radius could favour a special behavior of the dense particle cloud trapped in the discharge.

C. Discussion

A wide range of instabilities is observed in dusty and non-dusty plasmas. A possible explanation for the phenomenon observed here is the attachment induced ionization instabilities observed in low pressure RF discharges in electronegative gases [26, 27]. The main parameters responsible for these instabilities are the electron temperature T_e and density n_e. In fact, instabilities need two conditions to appear. First, the attachment rate coefficient has to increase more rapidly than the ionization one with the electron temperature. Second, the electron and negative ion densities must be of the same order of magnitude. Thus a small increase in the electron density can be rapidly amplified through a decrease of the electron temperature. Nighan and Wiegand gave a criterion for the appearance of the instability

$$R = \frac{\partial k_a/\partial T_e}{\partial k_i/\partial T_e} \succ 1, \qquad (1)$$

where k_a and k_i are respectively the attachment and ionization coefficients [26].

As dust particles are charged, they behave like large negative ions. The instabilities we observed may therefore be related to attachment induced ionization instabilities. During the accumulation phase, the nanocrystallites have been shown to grow and accumulate in the gas phase [22]. Their concentration increases until it reaches a critical value from which the coalescence phase starts. This critical value has been measured to be around 10^{11} to 10^{12} cm^{-3} [6]. However less than 0.1% of the dust particles are charged by electron attachment. The concentration of negatively charged nanocrystallites is therefore of the same order of magnitude as the electron density, just before the instability. Furthermore the electron temperature has been shown to be constant and equal to 2 eV during the accumulation phase [4]. Figure 15 shows the time evolution of the electron density n_e measured by the microwave resonant cavity method for different gas temperatures. The first very narrow peak (shown in the insert) corresponds to the SiH_3^- ion formation. Those ions are the first nuclei involved in the particle formation. Then, the electron density remains constant during the accumulation phase. Just at the onset of the coalescence, a slight decrease of the electron density can be observed (see the circle in fig.15) while the ion density remains constant. That means that at the beginning of the instability k_a increases while k_i remains constant ($\partial k_i/\partial T_e \longrightarrow 0$). And so R becomes larger than one.

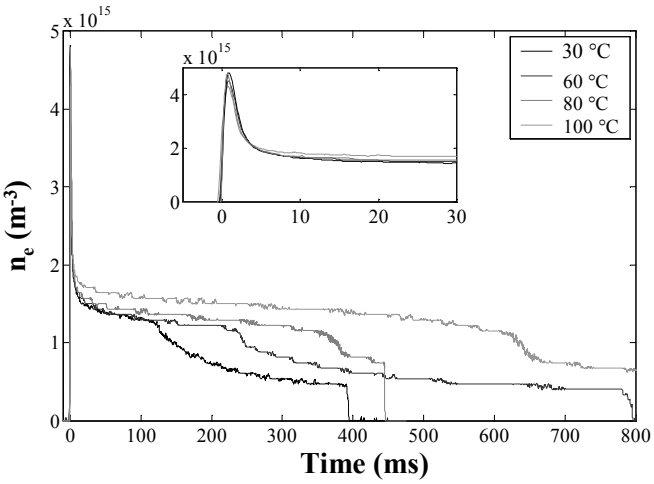

FIG. 15: (Color online) Time-evolution of the electron density for different gas temperatures. The insert is a zoom of the early beginning of the curve.

IV. CONCLUSION

In this paper we have presented new experimental results concerning a self-excited instability in silane based dusty plasma. These results have been obtained during particle nucleation and growth. We show that the instability has a complex form and that its frequency evolves in time. The effects of different parameters on the instability behavior are also reported, and a particular case has been evidenced. A possible explanation is also put forward thanks to a comparison with the instabilities observed in electronegative discharges. In the future, a comparison between the instabilities observed in [13] and those we observed will be investigated.

V. ACKNOWLEDGMENTS

The authors would like to thank Maurice Dudemaine and Sébastien Dozias for their help in electronics and Elizabeth Jolivet for her precious advice.

[1] L. Boufendi and A. Bouchoule, Plasma Sources Sci. Technol. **11**, A211 (2002).
[2] L. Boufendi, A. Bouchoule, and T. Hbid, J. Vac. Sci. Technol. A **14**, 572 (1995).
[3] J. Boeuf, Phys. Rev. A **46**, 7910 (1992).
[4] A. Fridman, L. Boufendi, T. Hbid, B. Potapkin, and A. Bouchoule, J. Appl. Phys. **79**, 1303 (1995).
[5] A. Bouchoule, A. Plain, L. Boufendi, J. Blondeau, and C. Laure, J. Appl. Phys. **70**, 1991 (1991).
[6] L. Boufendi, J. Gaudin, S. Huet, G. Viera, and M. Dudemaine, Appl. Phys. Lett. **49**, 4301 (2001).
[7] P. Roca i Cabarrocas, N. Chaabane, A. Kharchenko, and S. Tchakarov, Plasma Phys. Control. Fusion **46**, B235 (2004).
[8] P. Roca i Cabarrocas, Journal of Non-Crystalline Solids **1266-269**, 31 (2000).
[9] P. Roca i Cabarrocas, S. Kasouit, B. Kalache, R. Vanderhaghen, Y. Bonnassieux, M. Elyaakoubi, and I. French, Journal of the SID **12/1**, 1 (2004).
[10] G. Viera, M. Mikikian, E. Bertran, P. Roca i Cabarrocas, and L. Boufendi, J. Appl. Phys. **92**, 4684 (2002).
[11] G. Praburam and J. Goree, Phys. Plasmas **3**, 1212 (1996).
[12] D. Samsonov and J. Goree, Phys. Rev. E **59**, 1047 (1999).
[13] M. Mikikian and L. Boufendi, Phys. Plasmas **11**, 3733 (2004).
[14] M. Mikikian, M. Cavarroc, N. Chaumeix, and L. Boufendi, 31st EPS Conference on Plasma Phys. London ECA **28G**, O-2.13 (2004).
[15] A. Mezeghrane, M. Jouanny, M. Cavarroc, M. Mikikian, O. Lamrous, and L. Boufendi, 31st EPS Conference on Plasma Phys. London ECA **28G**, O-1.09 (2004).
[16] L. Boufendi, A. Plain, J. Blondeau, A. Bouchoule, C. Laure, and M. Toogood, Appl. Phys. Lett **60**, 169 (1992).
[17] L. Boufendi, A. Bouchoule, R. Porteous, J. Blondeau, A. Plain, and C. Laure, J. Appl. Phys. **73**, 2160 (1993).
[18] L. Boufendi, Ph.D. thesis, University of Orléans (1994).
[19] M. Shiratani, T. Fukuzawa, and Y. Watanabe, Jpn. J. Appl. Phys. **38**, 4542 (1999).
[20] P. Shukla and A. Mamun, *Introduction to Dusty Plasma Physics* (IoP, 2002).
[21] A. Bouchoule and L. Boufendi, Plasma Sources Sci. Technol. **3**, 292 (1994).
[22] L. Boufendi, J. Hermann, A. Bouchoule, B. Dubreuil, E. Stoffels, W. Stoffels, and M. de Giorgi, J. Appl. Phys. **76**, 148 (1994).
[23] U. Bhandarkar, U. Kortshagen, and S. L. Girshik, J. Phys. D : Appl. Phys. **36**, 1399 (2003).
[24] J. Perrin, O. Leroy, and M. Bordage, Plasma Phys. **36**, 1 (1996).
[25] J. Perrin, C. Bohm, R. Etemadi, and A. Lloret, Plasma Sources Sci. Technol. **3**, 252 (1994).
[26] W. Nighan and W. Wiegand, Phys. Rev. A **10**, 922 (1974).
[27] A. Descoeudres, L. Sansonnens, and C. Hollenstein, Plasma Sources Sci. Technol. **12** (2003).